THE JOURNAL OF BIOLOGICAL CHEMISTRY VOL. 284, NO. 30, pp. 20041–20051, July 24, 2009

Determinants in Ca_V1 Channels That Regulate the Ca^{2+} Sensitivity of Bound Calmodulin*[S]

Received for publication, April 25, 2009, and in revised form, May 19, 2009 Published, JBC Papers in Press, May 27, 2009, DOI 10.1074/jbc.M109.013326

D. Brent Halling[‡], Dimitra K. Georgiou[‡], D. J. Black[§], Guojun Yang[‡], Jennifer L. Fallon[‡¶], Florante A. Quiocho[‡¶], Steen E. Pedersen[‡], and Susan L. Hamilton[‡1]

From the [‡]Department of Molecular Physiology and Biophysics, Baylor College of Medicine, Houston, Texas 77030, the [§]Division of Molecular Biology and Biochemistry, University of Missouri, Kansas City, Missouri 64110, and the [¶]Verna and Marrs McLean Department of Biochemistry and Molecular Biology, Baylor College of Medicine, Houston, Texas 77030

Calmodulin binds to IQ motifs in the α_1 subunit of $Ca_V1.1$ and $Ca_V1.2$, but the affinities of calmodulin for the motif and for Ca^{2+} are higher when bound to $Ca_V1.2$ IQ. The $Ca_V1.1$ IQ and $Ca_V1.2$ IQ sequences differ by four amino acids. We determined the structure of calmodulin bound to $Ca_V1.1$ IQ and compared it with that of calmodulin bound to $Ca_V1.2$ IQ. Four methionines in Ca^{2+}-calmodulin form a hydrophobic binding pocket for the peptide, but only one of the four nonconserved amino acids (His-1532 of $Ca_V1.1$ and Tyr-1675 of $Ca_V1.2$) contacts this calmodulin pocket. However, Tyr-1675 in $Ca_V1.2$ contributes only modestly to the higher affinity of this peptide for calmodulin; the other three amino acids in $Ca_V1.2$ contribute significantly to the difference in the Ca^{2+} affinity of the bound calmodulin despite having no direct contact with calmodulin. Those residues appear to allow an interaction with calmodulin with one lobe Ca^{2+}-bound and one lobe Ca^{2+}-free. Our data also provide evidence for lobe-lobe interactions in calmodulin bound to $Ca_V1.2$.

The complexity of eukaryotic Ca^{2+} signaling arises from the ability of cells to respond differently to Ca^{2+} signals that vary in amplitude, duration, and location. A variety of mechanisms decode these signals to drive the appropriate physiological responses. The Ca^{2+} sensor for many of these physiological responses is the Ca^{2+}-binding protein calmodulin (CaM).[2] The primary sequence of CaM is tightly conserved in all eukaryotes, yet it binds and regulates a broad set of target proteins in response to Ca^{2+} binding. CaM has two domains that bind Ca^{2+} as follows: an amino-terminal domain (N-lobe) and a carboxyl-terminal domain (C-lobe) joined via a flexible α-helix. Each lobe of CaM binds two Ca^{2+} ions, and binding within each lobe is highly cooperative. The two lobes of CaM, however, have distinct Ca^{2+} binding properties; the C-lobe has higher Ca^{2+} affinity because of a slower rate of dissociation, whereas the N-lobe has weaker Ca^{2+} affinity and faster kinetics (1). CaM can also bind to some target proteins in both the presence and absence of Ca^{2+}, and the preassociation of CaM in low Ca^{2+} modulates the apparent Ca^{2+} affinity of both the amino-terminal and carboxyl-terminal lobes. Differences in the Ca^{2+} binding properties of the lobes and in the interaction sites of the amino- and carboxyl-terminal lobes enable CaM to decode local *versus* global Ca^{2+} signals (2).

Even though CaM is highly conserved, CaM target (or *recognition*) sites are quite heterogeneous. The ability of CaM to bind to very different targets is at least partially due to its flexibility, which allows it to assume different conformations when bound to different targets. CaM also binds to various targets in distinct Ca^{2+} saturation states as follows: Ca^{2+}-free (3), Ca^{2+} bound to only one of the two lobes, or fully Ca^{2+}-bound (4–7). In addition, CaM may bind with both lobes bound to a target (5, 6) or with only a single lobe engaged (8). If a target site can bind multiple conformers of CaM, CaM may undergo several transitions that depend on Ca^{2+} concentration, thereby tuning the functional response. Identification of stable intermediate states of CaM bound to individual targets will help to elucidate the steps involved in this fine-tuned control.

Both $Ca_V1.1$ and $Ca_V1.2$ belong to the L-type family of voltage-dependent Ca^{2+} channels, which bind apoCaM and Ca^{2+}-CaM at carboxyl-terminal recognition sites in their α_1 subunits (9–14). Ca^{2+} binding to CaM, bound to $Ca_V1.2$ produces Ca^{2+}-dependent facilitation (CDF) (14). Whether $Ca_V1.1$ undergoes CDF is not known. However, both $Ca_V1.2$ and $Ca_V1.1$ undergo Ca^{2+}- and CaM-dependent inactivation (CDI) (14, 15). $Ca_V1.1$ CDI is slower and more sensitive to buffering by 1,2-bis(*o*-aminophenoxy)ethane-*N*,*N*,*N*′,*N*′-tetraacetic acid than $Ca_V1.2$ CDI (15). Ca^{2+} buffers are thought to influence CDI and/or

* This work was supported, in whole or in part, by National Institutes of Health Grants AR44864 (to S. L. H.), HL087099 (to S. E. P.), and GM021371 (to F. A. Q.). This work was also supported by the Muscular Dystrophy Association (to S. L. H.) and Welch Foundation Grant Q-0581 (to F. A. Q.).

The atomic coordinates and structure factors (code 2vay) have been deposited in the Protein Data Bank, Research Collaboratory for Structural Bioinformatics, Rutgers University, New Brunswick, NJ (http://www.rcsb.org/).

[S] The on-line version of this article (available at http://www.jbc.org) contains data of CaM affinity for the mutant IQ peptides and the CD spectra of the IQ peptides $Ca_V1.1$ IQ, $Ca_V1.2$ IQ, $Ca_V1.1$ H1532Y, and $Ca_V1.2$ Y1675H.

[1] To whom correspondence should be addressed: Dept. of Molecular Physiology and Biophysics, Baylor College of Medicine, One Baylor Plaza, 410B, Houston, TX 77030. Tel.: 713-798-5704; Fax: 713-798-5441; E-mail: susanh@bcm.edu.

[2] The abbreviations used are: CaM, calmodulin; PDB, Protein Data Bank; N-lobe, amino-terminal domain of calmodulin; C-lobe, carboxy-terminal domain of calmodulin; RyR, ryanodine receptor; apoCaM, Ca^{2+}-free calmodulin; Ca^{2+}-CaM, calmodulin bound to four Ca^{2+}; CDF, Ca^{2+}-dependent facilitation; CDI, Ca^{2+}-dependent inactivation; MOPS, 3-(*N*-morpholino)propanesulfonic acid; r.m.s.d., root mean square deviation; IAEDANS, 5-((((2-iodoacetyl)amino)ethyl)amino)naphthalene-1-sulfonic acid; DDPM, *N*-(4-dimethylamino-3,5-dinitrophenyl)maleimide; FRET, fluorescence resonance energy transfer; SPR, surface plasmon resonance; CaM^{DA}, calmodulin labeled with donor and acceptor; CaM^{D}, calmodulin labeled with donor only.

CDF in voltage-dependent Ca^{2+} channels by competing with CaM for Ca^{2+} (16).

The conformation of the carboxyl terminus of the α_1 subunit is critical for channel function and has been proposed to regulate the gating machinery of the channel (17, 18). Several interactions of this region include intramolecular contacts with the pore inactivation machinery and intermolecular contacts with CaM kinase II and ryanodine receptors (17, 19–22). Ca^{2+} regulation of $Ca_V1.2$ may involve several motifs within this highly conserved region, including an EF hand motif and three contiguous CaM-binding sequences (10, 12). ApoCaM and Ca^{2+}-CaM-binding sites appear to overlap at the site designated as the "IQ motif" (9, 12, 13), which are critical for channel function at the molecular and cellular level (14, 23).

Differences in the rate at which 1,2-bis(*o*-aminophenoxy)ethane-*N,N,N′,N′*-tetraacetic acid affects CDI of $Ca_V1.1$ and $Ca_V1.2$ could reflect differences in their interactions with CaM. In this study we describe the differences in CaM interactions with the IQ motifs of the $Ca_V1.1$ and the $Ca_V1.2$ channels in terms of crystal structure, CaM affinity, and Ca^{2+} binding to CaM. We find the structures of Ca^{2+}-CaM-IQ complexes are similar except for a single amino acid change in the peptide that contributes to its affinity for CaM. We also find that the other three amino acids that differ in $Ca_V1.2$ and $Ca_V1.1$ contribute to the ability of $Ca_V1.2$ to bind a partially Ca^{2+}-saturated form of CaM.

EXPERIMENTAL PROCEDURES

Materials—All peptides used were either synthesized in the core facility at the Baylor College of Medicine under the direction of Dr. Richard Cook or by GenScript Corp. (Piscataway, NJ). $Ca_V1.1$ IQB and $Ca_V1.2$ IQB peptides had a six-carbon biotin linker attached via an additional modified lysine at the carboxyl terminus of the peptide (CPC Scientific Inc., San Jose, CA). Calibrated Ca^{2+} buffers were ordered through Invitrogen. High grade reagents for crystallization experiments were purchased from Hampton Research (Aliso Viejo, CA) or from Sigma. *N*-Trimethoxysilylpropyl-*N,N,N*-trimethylammonium chloride for silylizing glassware was purchased through United Chemical Technologies (Bristol, PA).

Mutant CaM Constructs—Fluorescent recombinant mammalian CaM constructs (F19W, F92W, and F92W/E12Q) were prepared as described previously (1, 24). Constructs for the mammalian Ca^{2+}-binding mutants E12QCaM and E34QCaM were also made previously (13). To prepare F19W/E34Q, we used a DNA construct for F19W in the pET3a vector. The cDNA primers (41 bp) were designed to introduce a glutamine substitution for a glutamate in the −z position of EF hands 3 and 4 (residues Glu-104 and Glu-140) by PCR site-directed mutagenesis. F19W/E12Q and F92W/E34Q were made similarly. Other mutants created using similar procedures included the following: 1) CaM mutants with cysteine mutations in the N-lobe (T34C) and the C-lobe (T110C); 2) E12Q/T34C/T110C; and 3) E34Q/T34C/T110C. The cDNA sequences were verified at the DNA Sequencing Core Facility at the Baylor College of Medicine. Protein expression and purification of these mutants were previously described (25).

TABLE 1
Data collection and refinement statistics for X-ray crystal structure

Data collection[a]	CaM/$Ca_V1.1$ IQ peptide
Wavelength	1.38079 Å
Maximum resolution	1.94 Å
Highest shell	2.06–1.94 Å
Total reflections	49,660
Unique reflections	15,915
Redundancy[b]	2.0 (1.7)
Completeness[b]	89.9% (51.0%)
$\langle I\rangle/\langle\sigma(I)\rangle^b$	3.65
$R_{sym}^{b,c}$	0.03 (0.205)
Refinement statistics	
R_{cryst}/R_{free}^{d}	0.228/0.285
Protein atoms/Ca^{2+}	1348/4
Water molecules	123
r.m.s.d. from ideal bond/angle	0.0096 Å/1.277°

[a] Crystal belongs to the C2 space group with one molecule in the asymmetric unit. The native domain crystal has unit cell dimensions of $a = 84.92$ Å, $b = 34.67$ Å, $c = 62.98$ Å, and $\alpha = 90°$, $\beta = 113.69$, $\gamma = 90°$.
[b] Values in parenthesis are for the highest resolution shell.
[c] $R_{sym} = \Sigma_{hkl}|I_{hkl} - \langle I_{hkl}\rangle|/\Sigma_{hkl}I_{hkl}$.
[d] R-factor $= \Sigma_{hkl}||F_o| - |F_c||/\Sigma_{hkl}|F_o|$, where $|F_o|$ and $|F_c|$ are the observed and calculated structure factor amplitudes for reflection hkl. R_{free} was calculated with a 10% subset of randomly chosen reflections not included in any stage of the refinement.

Preparation of Recombinant CaMs—Recombinant mammalian CaM protein (CaM wild type, F19W, F92W, and T34C/T110C) was purified for fluorescence analysis as described previously (26), except dithiothreitol (20 mM) and EGTA (2 mM) were included in lysis buffer for cysteine mutants, and 5 mM dithiothreitol was kept throughout purification steps. Ca^{2+}-binding mutants of CaM (T34C/T110C/E34Q and F19W/E34Q) were purified using a modified protocol from Rodney *et al.* (27).

Structure Determination—The complex of CaM-$Ca_V1.1$ IQ peptide complex was purified following the procedure described for the CaM-$Ca_V1.2$ IQ peptide complex (28). The complex was concentrated to 10 mg/ml in a buffer containing 20 mM MOPS, pH 7.4, 150 mM NaCl, and 10 mM $CaCl_2$. Crystals were grown by vapor diffusion by mixing 2 μl of complex into a 4-μl drop of a milieu from the well containing 32% polyethylene glycol 3500, 50 mM Tris, 50 mM $MgCl_2$. Large football-shaped crystals grew to full size in 2 weeks in a Torrey Pines Scientific incubator (San Marcos, CA) at 20 °C. Data were collected at the Center for Advanced Microstructures and Devices Gulf Coast Protein Crystallography Consortium beamline at the Louisiana State University Center for Advanced Microstructures and Devices (Baton Rouge, LA). The HKL2000 software package was used for data set reduction (29). The structure of CaM/$Ca_V1.1$ IQ was determined by the molecular replacement method (30) using the CaM/$Ca_V1.2$ IQ structure (PDB code 2f3y) (28) as the search model. The parameters used for solving the crystal structure are presented in Table 1. Structure refinement and analyses were performed using CNS (31) and the CHAIN graphics program (32). The structure was deposited to the Protein Data Bank (PDB) with the PDB code 2vay.

Determination of Affinity of CaM, E12QCaM, and E34QCaM for Peptides—Surface plasmon resonance (SPR) with a Biacore3000 instrument (GE Biacore, Inc., Piscataway, NJ) was used to assess the affinity of CaM, E12QCaM, and E34QCaM for the biotinylated wild type and mutant IQ peptides (Table 2). Sensor chip SA was conditioned according to the manufacturer's protocol, and biotinylated wild type or mutant IQ peptides were immobilized to a sensor chip SA by loading 100 μl of 3 nM

TABLE 2
Synthetic peptide sequences
Boldface is used for the amino acid that differs between the $Ca_V1.1$ IQ and $Ca_V1.2$ IQ peptides.

Accession no.	α_1 subunit	Sequence no.	Name	Sequence
Q13936	$Ca_V1.2$	1665–1685	$Ca_V1.2$ IQ	KFYATFLIQE**Y**FRKF**K**KR**K**E**Q**
Q13698	$Ca_V1.1$	1522–1542	$Ca_V1.1$ IQ	KFYATFLIQE**H**FRKF**M**KR**Q**E**E**
Mutant	$Ca_V1.2$		$Ca_V1.2$ Y1675H	KFYATFLIQEHFRKFKKRKEQ
Mutant	$Ca_V1.1$		$Ca_V1.1$ H1532Y	KFYATFLIQEYFRKFMKRQEE
Mutant	$Ca_V1.1$		$Ca_V1.1$/H1532Y/M1537K	KFYATFLIQEYFRKFKKRQEE
Mutant	$Ca_V1.1$		$Ca_V1.1$/H1532Y/Q1540K	KFYATFLIQEYFRKFMKRKEE
Mutant	$Ca_V1.1$		$Ca_V1.1$/H1532Y/E1542Q	KFYATFLIQEYFRKFMKRQEQ
Mutant	$Ca_V1.1$		$Ca_V1.1$/H1532Y/M1537K/Q1540K	KFYATFLIQEYFRKFKKRKEE
Biotinylated	$Ca_V1.2$		$Ca_V1.2$ IQB[a]	KFYATFLIQEYFRKFKKRKEQK$_c$-C6-biotin
Biotinylated	$Ca_V1.1$		$Ca_V1.1$ IQB[a]	KFYATFLIQEHFRKFMKRQEEK-C6-biotin
Biotinylated	$Ca_V1.2$		$Ca_V1.2$ Y1675H-IQB[a]	KFYATFLIQEHFRKFKKRKEQK-C6-biotin
Biotinylated	$Ca_V1.1$		$Ca_V1.1$ H1532Y-IQB[a]	KFYATFLIQEYFRKFMKRQEEK-C6-biotin

[a] Modified lysine residue was inserted to attach linker for biotin tag.

peptide in running buffer containing 3 mM $CaCl_2$, 30 mM MOPS, 100 mM KCl, 0.1 mg/ml BSA, 0.005% Tween 20, 0.02% NaN_3, pH 7.5, at a flow rate of 30 μl/min. Biotin (5–10 μl of 300 nM) alone was immobilized to control flow cells on the chip and used to subtract bulk movement of CaM, the analyte, to the chip during binding. Peptide immobilization was preceded and followed by a system desorb. CaM, E12QCaM, and E34QCaM were injected at a flow rate of 30 μl/min. All experiments were performed in triplicate; each sensorgram representing an independent dilution. K_D values were determined by fitting the amplitudes of the plateau phase as a function of CaM concentration using a one- or two-site saturation model.

Determination of Apparent Ca^{2+} Affinity of CaM Mutants with a Tryptophan Substitution—The procedure used was described by Black *et al.* (1). Data were fit by nonlinear regression analyses with either a standard dose-response curve or, if appropriate, a biphasic dose-response curve as modeled previously (1, 33).

Fluorescence Resonance Energy Transfer (FRET) of Labeled CaM—CaM with cysteine mutations at threonines 34 and 110 was purified and labeled with 5-((((2-iodoacetyl)amino)ethyl)-amino)naphthalene-1-sulfonic acid (1,5-IAEDANS) and *N*-(4-dimethylamino-3,5-dinitrophenyl) maleimide (DDPM), according to Xiong *et al.* (25). Only CaMs labeled with both IAEDANS and DDPM demonstrate FRET (25).

For FRET measurements, 200 nM labeled CaM was incubated with 1 μM peptide for 1 h at room temperature in a 20 μM Ca^{2+} buffer from Molecular Probes (Ca^{2+} calibration buffer kit 3). Fluorescence was measured at 400–625 nm with an SLM8000 spectrofluorometer with 350 nm excitation. Settings included 8-nm bandpass excitation and emission slits, 309 nm cut-on excitation filter, 395 nm cut-on emission filter, and 1-s integration times. All spectra had the same spectral maximum near 493 nm, and bar graphs reflect the observations at this wavelength.

Ca^{2+} Dissociation Kinetics—Stopped-flow experiments were performed as described (1, 24) using an Applied Photophysics instrument (model SX.18MV; Leatherhead, UK) to measure rates of Ca^{2+} dissociation (k_{off}) at 22 °C. Instrument parameters are the same as described (1). Represented data were averages of 5–8 individual traces fit with either a single or double exponential curve after premixing reached equilibrium. Tryptophan fluorescence was measured after rapidly mixing equal volumes (50 μl each) of solution A, F19WCaM or F92WCaM (4 μM), peptide (20 μM), and Ca^{2+} (200 μM) in 10 mM MOPS, 90 mM KCl, pH 7.0, with solution B, EGTA (10 mM). All traces were fit with the exponential Equation 1,

$$f = A*e^{-kt} + C \quad \text{(Eq. 1)}$$

where A is the amplitude of the fluorescence change, and k is the rate at which the change is occurring.

Ca^{2+} dissociation rates (1) were also determined with Quin-2. Solution A (CaM (8 μM), IQ peptide (40 μM), Ca^{2+} (15 μM) in 10 mM MOPS, and 90 mM KCl, pH 7.0) was rapidly mixed with an equal volume of solution B, Quin-2 (150 μM). The reaction was monitored by exciting fluorescence at 330 nm and measuring light emission with 510-nm broad bandpass filter (Oriel) in place. Quin-2 fluorescence traces required fits with the double exponential Equation 2,

$$f = A_1*e^{-k_1t} + A_2*e^{-k_2t} + C \quad \text{(Eq. 2)}$$

where A_1 and A_2 are component amplitudes of the fluorescence change, and k_1 and k_2 are the corresponding rates of change. The double exponential reflects the Ca^{2+} dissociation rates from both the N-lobe (fast) and the C-lobe (slow). The molar quantity of Ca^{2+} dissociating from CaM was calculated by monitoring the increase in Quin-2 fluorescence with increasing concentrations of Ca^{2+} standards (10, 20, 40, and 80 μM) (34).

RESULTS

Identification of IQ Residues That Interact Directly with Ca^{2+}-CaM—To define the determinants for interaction of $Ca_V1.1$ IQ and $Ca_V1.2$ IQ (differing by four amino acids) with CaM, we obtained crystals of Ca^{2+}-CaM bound to the $Ca_V1.1$ IQ peptide and determined the structure to 1.94 Å resolution (Table 1). The crystals are isomorphous to those formed with $Ca_V1.2$ IQ, and the crystal properties (Table 1) are very similar to those of the complex with $Ca_V1.2$ IQ peptide, but the CaM/$Ca_V1.2$ structure was determined at a higher resolution of 1.45 Å (28).

The N-lobe of CaM binds the amino terminus of the $Ca_V1.1$ IQ peptide, and the C-lobe binds the carboxyl terminus of $Ca_V1.1$ IQ in a parallel arrangement similar to that seen with $Ca_V1.2$ IQ (Fig. 1, *A* and *D*) and other IQ peptides (28, 35, 36). As expected from the identity of the amino-terminal portions of the $Ca_V1.1$ IQ and $Ca_V1.2$ IQ peptides, the N-lobe of CaM binds the amino-terminal peptide sequences in nearly identical

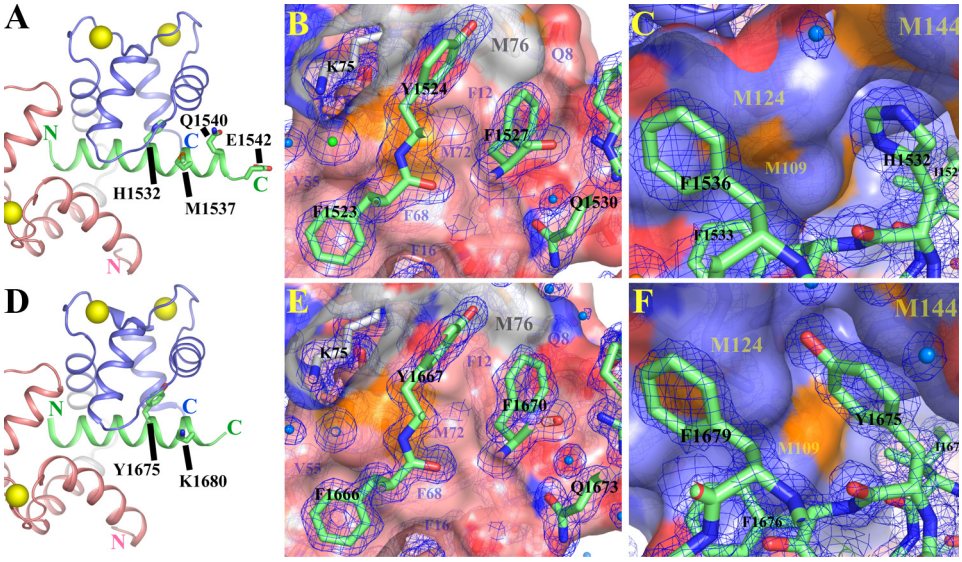

FIGURE 1. Structure of CaM bound to $Ca_V1.1$ IQ (PDB code 2vay) is represented in *A–C*. Structure of previously solved CaM bound to $Ca_V1.2$ IQ was obtained from the PDB with accession number 2f3y (*D–F*). *Ribbon* schematics represent CaM bound to $Ca_V1.1$ IQ in *A* or to $Ca_V1.2$ IQ in *D*. Peptides are represented as *green ribbons*. Ca^{2+} ions are represented as *yellow spheres*. The amino terminus (*N*) of the peptide contacts the N-lobe (*pink ribbon*) of CaM. C-lobe of CaM is *blue*. Linker ribbons that join the lobes of CaM are *light gray*. Residues of $Ca_V1.1$ IQ motif that are different from $Ca_V1.2$ IQ are represented as *sticks* on peptide ribbon, except for the residues not observed in the structure. *B* and *E* depict *peptide stick* residues contacting molecular surface of the N-lobe. *C* and *F* show peptide residue side chains (shown as *sticks*) in the vicinity of the C-lobe hydrophobic pocket formed by methionines (shown as molecular surface). *B, C, E,* and *F*, N-lobe carbons are *pink*, and carbon atoms in the linker between N- and C-lobes of CaM are *light gray*; C-lobe carbons are *light blue* (*teal*); peptide carbons are *green*; oxygen atoms are *red*; sulfur atoms are *orange*; nitrogen atoms are *dark blue*; waters are *marine spheres*; speculated chloride is *green sphere*. The $2F_o - F_c$ maps representing electron density are *blue meshes*. For best visibility, the 2vay $2F_o - F_c$ map is at 1.0 Å threshold and 2f3y map is at presented 0.5 Å.

conformations (Fig. 1, *B* and *E*). The root mean square deviation (r.m.s.d.) for the backbone atoms of the superimposed N-lobes is 0.34 Å. This value is about 2-fold smaller than the r.m.s.d. of 0.75 Å for the superimposed C-lobes, both of which are smaller than the overall backbone r.m.s.d. of 0.88 Å for the superimposed structures of the two CaM-peptide complexes. This indicates a difference in the relative orientation between the two lobes in the two structures.

Other differences are detected in the C-lobe interactions. There is a salt bridge between Arg-1539 on the $Ca_V1.1$ IQ peptide and Glu-127 of CaM that was not observed in our $Ca_V1.2$ IQ-CaM structure (28), but it was seen in the structure by Van Petegem *et al.* (36). Of the four nonconserved residues, only His-1532 on $Ca_V1.1$ IQ (Fig. 1, *A* and *C*) and Tyr-1675 in $Ca_V1.2$ IQ (Fig. 1, *D* and *F*) contact Ca^{2+}-CaM. In Ca^{2+}-CaM/$Ca_V1.2$ IQ, a water molecule forms hydrogen bonds both with the hydroxyl group side chain of the Tyr-1675 and with the carbonyl oxygen of the Met-124 main chain (28). A hydrophobic pocket formed by four C-lobe methionine side chains is more collapsed around His-1532 (Fig. 1*C*). This Ca^{2+}-CaM methionine pocket expands around the bulkier Tyr-1675 on the $Ca_V1.2$ IQ peptide (Fig. 1*F*). Although the methionine side chains are slightly farther away from Tyr-1675, the α-carbon atoms are actually drawn inward toward the tyrosine. When comparing structures, the main chain α-carbon atoms of residues of Met-109, Met-124, Met-144, and Met-145 are displaced by 0.54, 0.18, 0.52, and 0.38 Å, respectively. The α-carbon to α-carbon distance from Met-109 to Met-145 is 0.41 Å closer in the presence of $Ca_V1.2$ IQ than in the presence of $Ca_V1.1$ IQ. The α-carbons are 0.12 Å closer from Met-124 to Met-144. The difference in α-carbon positions correlates with small perturbations in backbone structure. As mentioned above, the r.m.s.d. of the C-lobes from both complexes is 0.75 Å, but it is influenced mainly by the difference in the relative positions of the α6-α7 loops; the r.m.s.d. measured without the α6-α7 loop drops to 0.63 Å. Because 0.63 Å is still considerably larger than the r.m.s.d. of the N-lobes, it likely reflects variations in the C-lobe conformations caused by the different peptides.

Because the pH of the crystallization solution is 8.3, His-1532 of $Ca_V1.1$ IQ is likely in the neutral or nonprotonated form. A charged residue in this position is predicted to be unfavorable. To assess this, we created peptides with an H1532D replacement in $Ca_V1.1$ IQ. This peptide does not bind Ca^{2+}-CaM (data not shown), suggesting that the residue in this position (His-1532 of $Ca_V1.1$ IQ or Tyr-1675 of $Ca_V1.2$ IQ) is important for the interactions within the methionine pocket. A useful side note is that the H1532D mutation in $Ca_V1.1$ can be used to abolish CaM binding.

How Nonconserved Amino Acids in IQ Motif Regulate the Affinity for Ca^{2+}-CaM—To address the question of how the four nonconserved amino acids affect the affinity of the IQ peptides for Ca^{2+}-CaM, we synthesized the peptides shown in Table 2 and assessed their affinity using SPR. $Ca_V1.1$ IQ, $Ca_V1.2$ IQ, $Ca_V1.2$ Y1675H, $Ca_V1.1$ H1532Y, and four $Ca_V1.1$ mutant peptide with the H1532Y substitution and one or more amino acid changes were tested. Briefly, we assessed the affinity of the biotinylated wild type and mutant IQ peptides listed in Table 2 for Ca^{2+}-CaM in saturating Ca^{2+} concentrations. We also performed competition experiments for CaM binding to immobilized biotinylated peptides using increasing concentrations of the nonbiotinylated peptides listed in Table 2 (see supporting information). Binding data reflecting the interaction of Ca^{2+}-CaM with the biotinylated peptides are shown in Fig. 2. The interactions are adequately modeled with a simple bimolecular interaction for the concentration range shown in Fig. 2, with a K_D of 7.9 nM for the $Ca_V1.1$ IQB, 2.5 nM for the $Ca_V1.2$ IQB, 4 nM for the $Ca_V1.1$ H1532Y-IQB, and 2.9 nM for the $Ca_V1.2$ Y1675H-IQB. This finding suggests that at low concentrations (<50 nM approximately) CaM assumes one binding conformation to the IQ peptides. As concentration increases, the data are fitted better to the two site saturation model (data not shown), suggesting that at higher concentrations CaM binds in two or more different conformations to the IQ peptides. For simplicity, we have chosen to compare only the high affinity interac-

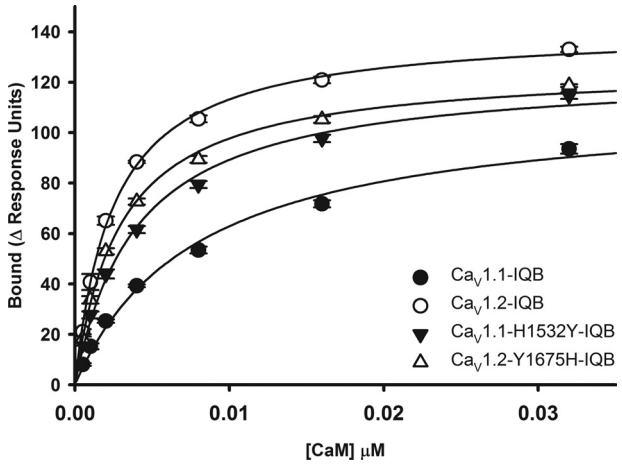

FIGURE 2. **Affinity of CaM for biotinylated wild type and mutant IQ peptides.** CaM binding to peptides $Ca_V1.1$ IQB, $Ca_V1.2$ IQB, $Ca_V1.1$ H1532Y-IQB, and $Ca_V1.2$ Y1675H-IQB is shown. The *solid lines* represent the fits to one site saturation model. The K_D values are 7.9 ± 1.1 nM for $Ca_V1.1$ IQ, 2.5 ± 0.1 nM for $Ca_V1.2$ IQ, 4.0 ± 0.4 nM for $Ca_V1.1$ H1532Y-IQB, and 2.9 ± 0.2 nM for $Ca_V1.2$ Y1675H-IQB. Each data point represents the mean ± S.E. for three independent experiments.

tions. The H1532Y mutation in $Ca_V1.1$ IQ increases the affinity for CaM, but the affinity is still lower than that of $Ca_V1.2$ IQ. The Y1675H mutation in $Ca_V1.2$ IQ results in only a decrease in CaM affinity. These findings together with the competition data with the other mutant peptides (see supporting information) suggest that all four amino acids that differ between the peptides contribute to the overall affinity for CaM, despite the finding that only one of them interacts with CaM in the crystal structure, suggesting that the interactions detected in the crystal are not the only interactions that occur in solution.

Amino Acids in the IQ Motif That Regulate the Ca^{2+} Affinity of Bound CaM—The primary function of CaM is to transduce a Ca^{2+} signal into a protein response. The apparent affinity of CaM for Ca^{2+} in the presence of a target peptide is coupled to the affinity of CaM for the peptide. In addition, an interaction of apoCaM (Ca^{2+}-free CaM) with an IQ peptide can increase the apparent Ca^{2+} affinity of CaM by altering the conformation of the Ca^{2+}-binding sites. Tryptophan mutants of CaM have been used to assess apparent Ca^{2+} affinity to CaM complexed to peptides (24). The apparent Ca^{2+} affinity of CaM, referred to here as $K_{D,app}$, is determined from the Ca^{2+} titration of the tryptophan fluorescence. F19W is a CaM mutant that indirectly measures Ca^{2+} binding to the N-lobe, and the interaction of $Ca_V1.2$ IQ with F19W increases its Ca^{2+} affinity (1). The apparent Ca^{2+} affinity of the N-lobe of F19W complexed to $Ca_V1.1$ IQ (254 nM) is less than that of the N-lobe of F19W bound to $Ca_V1.2$ IQ (49 nM) (Fig. 3*A* and Table 3) (1). We used F92WCaM to assess Ca^{2+} binding to the C-lobe. The Ca^{2+} titration of the fluorescence of the C-lobe of F92W was fit with a single component for $Ca_V1.1$ but was distinctly biphasic with $Ca_V1.2$ (1), as characterized by a Ca^{2+}-dependent increase followed by a decrease in fluorescence. The decrease in fluorescence with F92W/$Ca_V1.2$ IQ at higher Ca^{2+} concentrations is likely to be due to the N-lobe quenching the fluorescence of the C-lobe upon binding Ca^{2+}. The discrepancy between the N-lobe Ca^{2+} affinity determined with $Ca_V1.2$ and F19W (49 nM) and that estimated from the quenching (198 nM) is likely to be due to the difficulty in fitting this complex biphasic curve. In these experiments the peptide is present in a 5-fold molar excess over CaM, and therefore, two CaMs binding to a single peptide is not likely. Overall, the Ca^{2+} affinity of the C-lobe of F92W complexed to $Ca_V1.2$ IQ is about 5-fold higher than that of the C-lobe of F92W bound to $Ca_V1.1$ IQ, a factor that is similar to the change observed at the N-lobe (Fig. 3*B* and Table 3).

Identification of the Amino Acids Responsible for the Higher Ca^{2+} Affinity of CaM Bound to $Ca_V1.2$—As mentioned previously, of the four nonconserved amino acids, only His-1532 in $Ca_V1.1$ IQ and Tyr-1675 in $Ca_V1.2$ actually contact Ca^{2+}-CaM in the crystal structures (Fig. 1). If the residue at this position in the IQ motifs is responsible for the difference in Ca^{2+} affinity of CaM bound to $Ca_V1.2$ *versus* $Ca_V1.1$, it should be possible to lower the Ca^{2+} affinity of $Ca_V1.2$ IQ by converting Tyr-1675 to a His and to increase the Ca^{2+} affinity of $Ca_V1.1$ IQ by converting His-1532 to a Tyr. The peptides with amino acids substitutions used in this study are listed in Table 2. The apparent N-lobe Ca^{2+} affinity of F19W bound to $Ca_V1.1$ H1532Y is only slightly different from that of F19W bound to $Ca_V1.1$ IQ, suggesting that this residue alone is not responsible for the higher Ca^{2+} affinity of the N-lobe of F19W bound to $Ca_V1.2$ IQ (Fig. 3*C*). The apparent N-lobe Ca^{2+} affinity of F19W bound to $Ca_V1.2$ Y1675H is less than that of F19W bound to $Ca_V1.2$ IQ, but it is still higher than that of F19W bound to $Ca_V1.1$ IQ. With F92W to monitor Ca^{2+} affinity of the C-lobe, the first obvious difference using $Ca_V1.2$ Y1675H is the absence of the fluorescence quenching seen at higher Ca^{2+} concentrations with $Ca_V1.2$ IQ and F92W (Fig. 3*D*). This suggests that the lobes may not be in close enough proximity when bound to the $Ca_V1.2$ Y1675H peptide to cause quenching. The Y1675H substitution does reduce the Ca^{2+} affinity of the C-lobe of the F92W (Fig. 3, *B* and *D*, and Table 3). These data suggest that the amino acids at this position influence the Ca^{2+} affinities of both lobes of CaM but cannot alone account for the difference in Ca^{2+} affinities of CaM bound to $Ca_V1.1$ IQ and $Ca_V1.2$ IQ. The other nonconserved amino acids, despite their lack of contact with Ca^{2+}-CaM in the crystal structure, must be contributing to these observed differences.

Lys-1680, Lys-1683, and Gln-1685 provide $Ca_V1.2$ IQ with a +3 net charge compared with $Ca_V1.1$ IQ. Four peptides, each containing the H1532Y substitution in $Ca_V1.1$ and one or more of the above amino acid changes (Table 2), were tested for effects on the Ca^{2+} affinity of bound F19WCaM and F92WCaM. All of these peptides increased the apparent Ca^{2+} affinity of both F19W and F92W relative to these CaMs complexed to either $Ca_V1.1$ IQ or $Ca_V1.1$ H1532Y (highest p value = 0.0017) (Fig. 3, *E* and *F*, and Table 3). The most dramatic changes were seen with $Ca_V1.1$/H1532Y/M1537K and $Ca_V1.1$/.H1532Y/M1537K/Q1540K. These data suggest that all of the nonconserved residues modulate the Ca^{2+} affinity of both lobes of CaM.

Partially Ca^{2+}-saturated CaM Binds with Both Lobes to $Ca_V1.2$ IQ—One explanation of the observation that amino acids that do not interact with Ca^{2+}-CaM in the crystal increase Ca^{2+} affinity is that these amino acids are involved in the binding of CaM in a Ca^{2+}-free or a partially Ca^{2+}-saturated state.

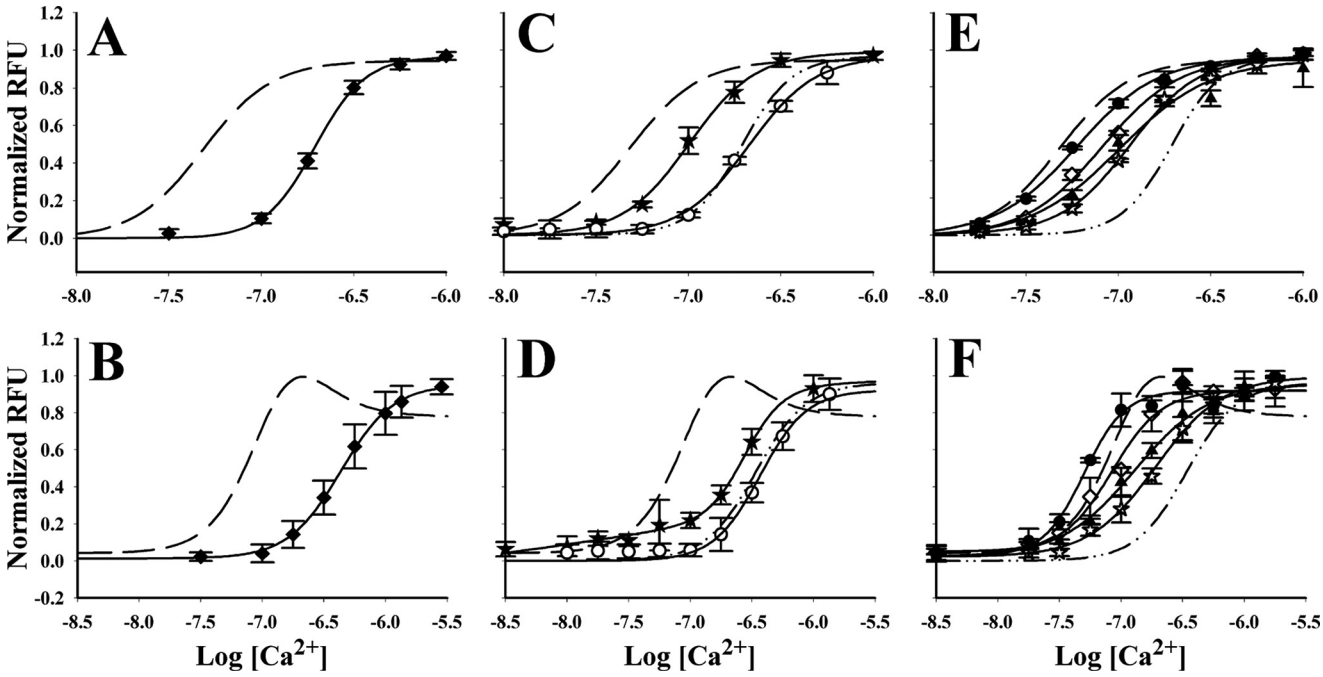

FIGURE 3. **Effect $Ca_V1.1$ IQ peptides on Ca^{2+} affinity of CaM mutants with tryptophan reporters.** Normalized relative fluorescence units (*RFU*) from 1 μM tryptophan mutant CaM and 5 μM peptide are plotted as the mean ± S.D. from three independent trials. *A, C,* and *E* contain normalized fluorescence data for F19W; and *B, D,* and *F* contain data for F92W. In all panels, data describing Ca^{2+} binding to tryptophan mutant CaM complexed with $Ca_V1.2$ IQ peptide were presented before in Black *et al.* (1), but the fits from F19W/$Ca_V1.2$ IQ are represented by a *dashed line* in *A, C,* and *E*; or the fit from F92W/$Ca_V1.2$ IQ are represented by a *dashed line* in *B, D,* and *F*. *A* and *B,* CaM/$Ca_V1.1$ IQ, *closed diamonds*. *C* and *D, closed star,* CaM/$Ca_V1.2$ Y1675H; and *open circles,* CaM/$Ca_V1.1$ H1532Y. *Dash-dot-dot trace* represents the curve fitted CaM/$Ca_V1.1$ IQ in *A* and *B* for F19W and F92W, respectively. Data for F92W/$Ca_V1.2$ Y1675H were fit with a biphasic sigmoid curve. *E* and *F, open diamond,* $Ca_V1.1$/H1532Y/M1537K; *closed triangle,* $Ca_V1.1$/H1532Y/Q1540K; *open star,* $Ca_V1.1$/H1532Y/E1542Q; and *closed circle,* $Ca_V1.1$/H1532Y/M1537K/Q1540K. *Dash-dot-dot traces* for *E* and *F* are the same as in *C* and *D,* respectively.

TABLE 3

CaM $K_{D,app}$ for Ca^{2+} in presence of peptides determined from analyses of fluorescence from CaM containing tryptophan substitutions

Superscript numbers 1–4 are used to mark the values that are compared through the *p* values that are given in the last two rows in table.

	F19W $K_{D,app}$	Hill coefficient	F92W $K_{D,app}$	Hill coefficient
	nM		*nM*	
No peptide	4840 ± 700	3.0 ± 0.9	1,400 ± 153	1.8 ± 0.1
$Ca_V1.1$ IQ	[1]254 ± 12	3.1 ± 0.3	[1]540 ± 33	1.9 ± 0.2
$Ca_V1.2$ IQ	[2]49 ± 3	2.4 ± 0.2	104 ± 9	1.8 ± 0.2
			198 ± 51	2.2 ± 0.3
$Ca_V1.1$ H1532Y	[3]213 ± 11	2.6 ± 0.3	[2]400 ± 40	3.3 ± 0.4
$Ca_V1.2$ Y1675H	[4]104 ± 7	2.6 ± 0.4	250 ± 20	1.7 ± 0.4
$Ca_V1.1$/H1532Y/M1537K	82 ± 1	2.1 ± 0.1	[3]84 ± 10	2.2 ± 0.4
$Ca_V1.1$/H1532Y/Q1540K	102 ± 5	1.8 ± 0.1	135 ± 22	1.5 ± 0.4
$Ca_V1.1$/H1532Y/E1542Q	115 ± 2	2.4 ± 0.1	193 ± 26	1.6 ± 0.1
$Ca_V1.1$/H1532Y/M1537K/Q1540K	60 ± 1	1.9 ± 0.1	[4]50 ± 2	2.6 ± 0.7
p value for 1–2, 2–4, 1–4	<0.0003	*p* value for 1–2	0.0003	
p value for 1–3	0.01	*p* value for 1–3, 1–4	0.0001	

This type of interaction could increase the apparent Ca^{2+} affinity of the sites by altering the conformation of the Ca^{2+}-free sites. We used Ca^{2+}-binding site mutants of CaM, FRET analyses, and measurement of Ca^{2+} dissociation rates to determine whether $Ca_V1.2$ and $Ca_V1.1$ have different abilities to bind CaM with one lobe Ca^{2+}-bound and one lobe Ca^{2+}-free.

To assess the effects of Ca^{2+} binding at one lobe of CaM on the Ca^{2+} binding properties of the second lobe, we created a series of CaM mutants (F19W/E34Q, F92W/E12Q, F19W/E12Q, and F92W/E34Q) that combined the tryptophan substitutions with mutations in either the N- or C-lobe Ca^{2+}-binding sites. As shown previously with *Drosophila* CaM, the E12Q mutation (glutamates in the −z positions of EF hands 1 and 2 are mutated to glutamines) abolishes Ca^{2+} binding to the N-lobe, and the E34Q mutation (glutamates in the −z positions of EF hands 3 and 4 are mutated to glutamines) abolishes Ca^{2+} binding to the C-lobe (37). The F19W/E34Q and F92W/E12Q mutants are used to detect Ca^{2+} binding to the N- and C-lobes, respectively. Mutations in the Ca^{2+}-binding sites in the C-lobe decreased the apparent Ca^{2+} affinity of the N-lobe, whereas mutations in the N-lobe had lesser effects on the apparent Ca^{2+} affinity of the C-lobe bound to $Ca_V1.2$ (Fig. 4*A* and Table 4). The apparent Ca^{2+} affinity of F19W/E34Q when bound to $Ca_V1.2$ IQ ($K_{D,app}$ for Ca^{2+} = 208 nM) is greater than when bound to $Ca_V1.1$ IQ ($K_{D,app}$ for Ca^{2+} = 690 nM) (Fig. 4*A* and Table 4). These values demonstrate lower affinities than obtained with F19WCaM complexed to $Ca_V1.2$ IQ (50 nM) and $Ca_V1.1$ IQ (190 nM) and are likely to reflect both the contributions of the other lobe and the decreased affinity of the Ca^{2+}-binding site mutants of CaM for the peptide. The

Ca^{2+} titration of the tryptophan fluorescence of F92W/E12Q CaM-$Ca_V1.2$ IQ is monophasic with increasing Ca^{2+} concentrations with a $K_{D,app}$ of 135 nM (Table 4) (1). F92W/E12Q complexed to $Ca_V1.1$ displays a $K_{D,app}$ for Ca^{2+} of 790 nM (Fig. 4*B* and Table 4).

We used two additional mutants as follows: the F19W/E12Q to detect alterations in Ca^{2+} free N-lobe arising from Ca^{2+} binding to the C-lobe, and F92W/E34Q to detect alterations in Ca^{2+}-free C-lobe arising from Ca^{2+} binding to the N-lobe. We were unable to detect Ca^{2+}-dependent fluorescence changes with F19W/E12Q and F92W/E34Q either in the absence of peptide or with $Ca_V1.1$ IQ. However, we were able to detect Ca^{2+}-dependent changes in fluorescence of both F19W/E12Q and F92W/E34Q in complex with $Ca_V1.2$ IQ. The $K_{D,app}$ for Ca^{2+} for F19W/E12QCaM-$Ca_V1.2$ IQ was 21 nM, whereas that of F19W/E12QCaM-$Ca_V1.2$ IQ was 120 nM. These findings suggest that Ca^{2+} binding to either the N- or C-lobe of CaM changes the environment of the tryptophan in the Ca^{2+}-free lobe, suggesting an interaction between lobes when CaM is bound to $Ca_V1.2$. In both cases the apparent affinity was higher when the tryptophan was in the Ca^{2+}-free lobe suggesting that a tryptophan in the Ca^{2+}-free lobe either facilitates the interaction between the lobes or increases the affinity of the Ca^{2+}-free lobe for $Ca_V1.2$. Either explanation would support a lobe-lobe interaction when CaM is bound to $Ca_V1.2$.

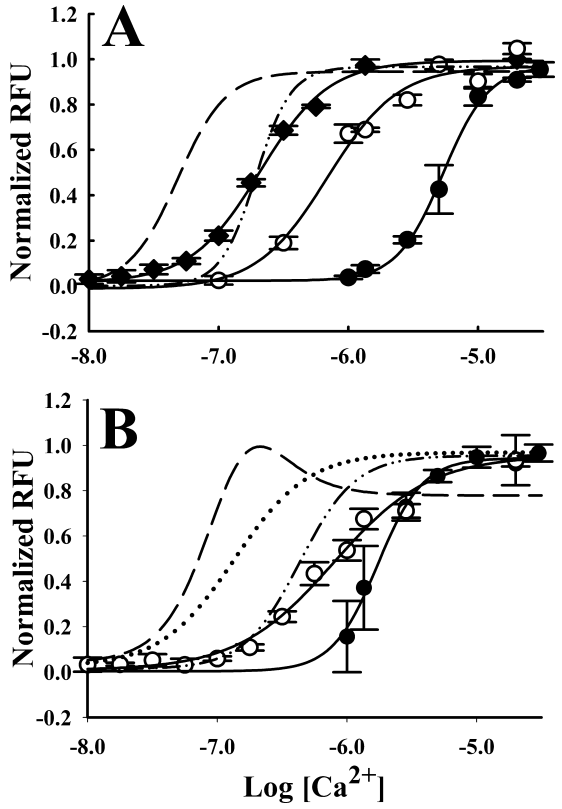

FIGURE 4. **Effect of blocking Ca^{2+} binding to a single lobe on the $K_{D,app}$ of CaM for Ca^{2+} when bound to peptide.** All data were collected in triplicate as the mean ± S.D. *A*, 1 μM F19W/E34Q alone (*closed circles*) or with 5 μM $Ca_V1.1$ IQ (*open circles*) or with 5 μM $Ca_V1.2$ IQ (*closed diamonds*). All data are fit with standard sigmoid curve. *Long dashes*, fit for F19W/$Ca_V1.2$ IQ shown previously (1); *dash-dot-dot*, fit for F19W/$Ca_V1.1$ IQ from Fig. 3. *B*, 1 μM F92W/E12Q alone (*closed circles*) or with 5 μM $Ca_V1.1$ IQ (*open circles*) are plotted. *Long dashes*, fit for F92W/$Ca_V1.2$ IQ shown previously (1); *dash-dot-dot*, fit for F92W/$Ca_V1.1$ IQ from Fig. 3; *dotted line*, fit for F92WE12Q/$Ca_V1.2$ IQ shown previously (1).

To further support the interaction of partially saturated CaM with $Ca_V1.2$, we used stopped-flow fluorescence measurements and the F19W and F92W mutants to measure the rate of Ca^{2+} dissociation from each lobe of CaM in the presence of the peptides. The tryptophan mutations in F19W and F92W have only small effects on Ca^{2+} dissociation rates compared with unmodified CaM (1). Similar experiments have previously shown that Ca^{2+} dissociates from the N-lobe faster than from the C-lobe of CaM and that the binding of CaM to peptides slows the rate of Ca^{2+} dissociation from both lobes (1). The interaction with $Ca_V1.1$ also slows Ca^{2+} dissociation from F19W and F92WCaM (Fig. 5). Using F19W we found that the rate of dissociation from the N-lobe was similar when F19W was bound to $Ca_V1.1$ IQ (6.3 s^{-1}) and $Ca_V1.2$ IQ (6.4 s^{-1}) (Fig. 5*A* and Table 5). Initial Ca^{2+} dissociation is modestly faster from the C-lobe (F92W) when bound to $Ca_V1.1$ IQ (k_d = 1.3 s^{-1}) compared with $Ca_V1.2$ IQ (0.8 s^{-1}) (Fig. 5*B* and Table 5). However, F92W complexed to $Ca_V1.2$ IQ (but not $Ca_V1.1$ IQ) displays a two component dissociation (1). The fluorescence first increases and then decreases. These data demonstrate that the tryptophan in the F92WCaM-$Ca_V1.2$ IQ complex can detect a conformational change in the N-lobe as it releases Ca^{2+} and that a stable intermediate with CaM with its N-lobe Ca^{2+} free can be detected kinetically. It is possible that CaM also binds $Ca_V1.1$ IQ with one lobe Ca^{2+}-free, but the biphasic dissociation is too fast to detect in these experiments.

We also measured Ca^{2+} dissociation rates using stopped-flow kinetics and the fluorescent Ca^{2+} chelator Quin-2. With Quin-2, fluorescence increases when it binds Ca^{2+}. In the absence of peptide, the rate of increase in Quin-2 fluorescence can be fit with a single exponential because the N-lobe Ca^{2+} dissociation is too fast to be resolved by Quin-2 (represented as a *dotted line* in Fig. 5*C* from data presented in Ref. 1). In the presence of $Ca_V1.2$ IQ peptide, however, a double exponential dissociation is detected (represented as *dashed line* in Fig. 5*C* as performed in Ref. 1). The kinetic constants are similar to those obtained with F19W and F92W (1). We measured the rate of Ca^{2+} dissociation from CaM in the presence of the $Ca_V1.1$ IQ

TABLE 4

Effects of Ca^{2+}-binding site mutations on the Ca^{2+} affinity of the lobes of CaM

NF indicates no fluorescence change.

	F19W/E34Q, $K_{D,app}$	Hill no.	F92W/E12Q, $K_{D,app}$	Hill no.	F19W/E12Q, $K_{D,app}$	Hill no.	F92W/E34Q, $K_{D,app}$	Hill no.
Ca^{2+}-binding lobe	N-lobe		C-lobe		C-lobe		N-lobe	
No peptide	5400 ± 700	2.6 ± 0.3	1700 ± 500	2.5 ± 0.8	NF	NF	NF	NF
$Ca_V1.1$ IQ	690 ± 30	1.6 ± 0.1	790 ± 70	1.2 ± 0.1	NF	NF	NF	NF
$Ca_V1.2$ IQ	208 ± 7[a]	1.6 ± 0.1	135 ± 6	1.5 ± 0.3	21 ± 10	2.0 ± 1	120 ± 42	1.5 ± 0.5

[a] p value = 0.00001.

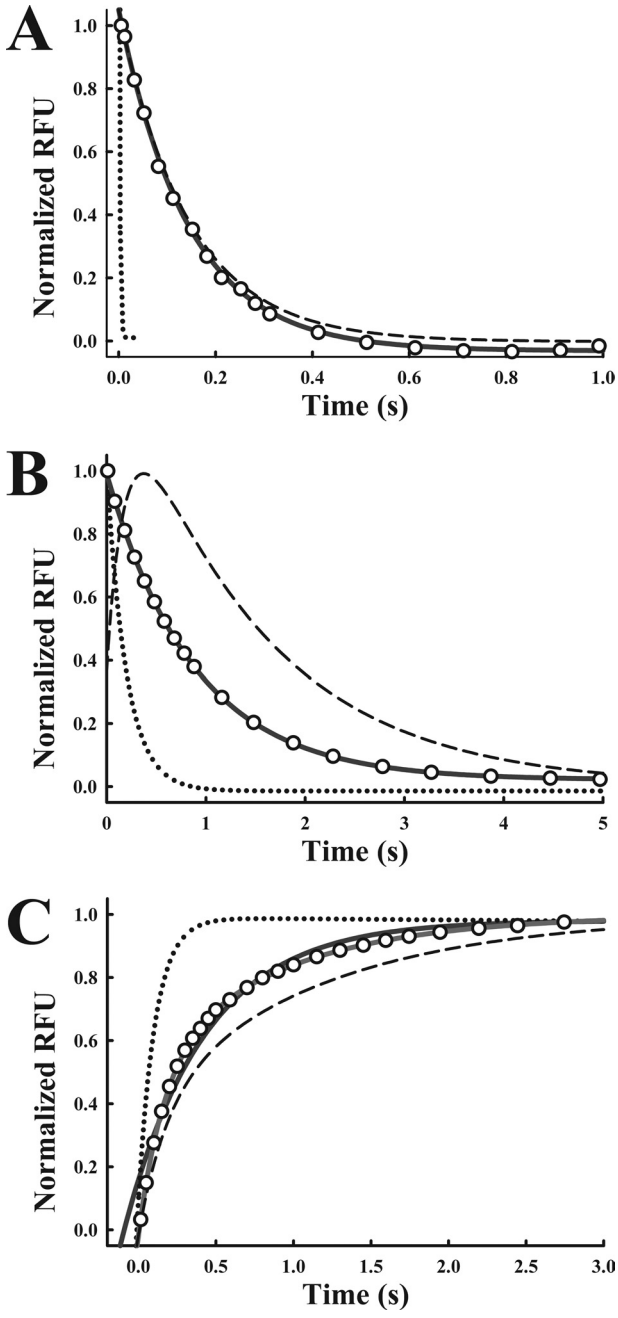

FIGURE 5. **Ca^{2+} dissociation from CaM is faster when it is bound to $Ca_V1.1$ IQ peptide than when bound to $Ca_V1.2$ IQ.** *A, dotted line* and *dashed line* represent fits to data that were published previously showing F19W alone and F19W/$Ca_V1.2$ IQ, respectively (1). New data showing Ca^{2+} dissociation from F19W bound to $Ca_V1.1$ IQ are represented by *open circles*. For clarity in comparing fits, only ~5% of the total data points are plotted. Data are normalized to maximum and minimum fluorescence. *Gray solid line* represents a fit with a single exponential. *B, dotted line* and *dashed line* represent fits to data that were published previously showing F92W alone and F92W/$Ca_V1.2$ IQ, respectively (1). New data showing Ca^{2+} dissociation from F92W bound to $Ca_V1.1$ IQ are represented by *open circles*. Only ~5% total data displayed for clarity in comparing fits. *Gray solid line* is single exponential fit. *C,* Quin-2 fluorescence increases as Ca^{2+} dissociates from CaM. *Dotted line* and *dashed line* are fits to data that were published previously showing CaM alone and CaM/$Ca_V1.2$ IQ, respectively (1). ~5% of collected data for CaM in presence of $Ca_V1.1$ IQ peptide are shown as *open circles*. The *gray solid line* representing a single exponential fit does not fit as well as the *black solid line* representing a double exponential fit (Rsqr 0.9776, *gray*; 0.9999, *black*).

TABLE 5
Ca^{2+} dissociation rates from CaM in presence of peptides

	Ca^{2+} dissociation rate via (CaM-Trp) mutants		Ca^{2+} dissociation rate via Quin-2	
	F19W k_d	F92W k_d	k_{d1}	k_{d2}
	s^{-1}	s^{-1}	s^{-1}	s^{-1}
No peptide[a]	*650*	*5.0*	*>1000*	*7.5*
$Ca_V1.1$[b]	6.3 ± 0.2	1.3 ± 0.1	6.4 ± 0.3	1.4 ± 0.2
$Ca_V1.2$[a,b]	*6.4*	*0.8*	*5.6*	*0.9*
p value[b]		0.0036	0.0006	0.0179

[a] Italicized data were published previously (1).
[b] *p* values are as shown.

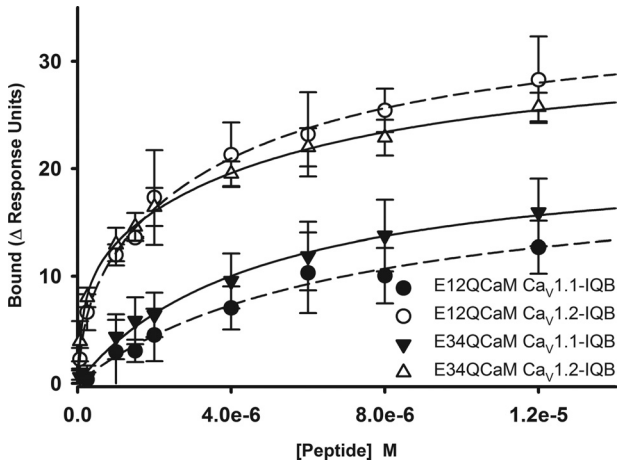

FIGURE 6. **Affinity of E12QCaM and E34QCaM for the IQ peptides.** Data of E12QCaM binding to $Ca_V1.1$ IQB and $Ca_V1.2$ IQB and E34QCaM binding to $Ca_V1.1$ IQB and $Ca_V1.2$ IQB are presented. Each data point represents the mean ± S.D. The *lines* represent the one and two component fits for the $Ca_V1.1$ IQ and $Ca_V1.2$ IQ, respectively. The K_D values for $Ca_V1.1$ IQB-E12QCaM and $Ca_V1.1$ IQB-E34QCaM interactions are 6950 ± 1427 and 4694 ± 540 nM, respectively, and for $Ca_V1.2$ IQB-E12QCaM are 4366 ± 2283 and 197 ± 157 nM and $Ca_V1.2$ IQB-E34QCaM are 5745 ± 1626 and 137 ± 32 nM.

peptide. As expected from the tryptophan fluorescence studies, Ca^{2+} dissociates faster from CaM when bound to $Ca_V1.1$ IQ than when bound to $Ca_V1.2$ IQ (Fig. 5*C* and Table 5). The Quin-2 data also support the existence of a stable intermediate with partially saturated CaM in complex with $Ca_V1.2$.

Peptide Binding Affinity of Partially Ca^{2+}-saturated CaM—The lobe-lobe interactions of CaM bound to $Ca_V1.2$ raise the issue of Ca^{2+} binding affinities of CaM lobes. We address this issue by assessing the affinity of the biotinylated wild type IQ peptides for E12QCaM and E34QCaM in saturating Ca^{2+} concentrations using SPR (Fig. 6). The interactions of E12QCaM and E34QCaM with the $Ca_V1.1$ IQB peptide are fit to a one-site saturation model with a K_D of 6950 and 4695 nM, respectively, whereas the interactions with $Ca_V1.2$ IQB are fit to a two-site saturation model with K_D values of 4366 and 197 nM for interaction with E12QCaM and K_D values of 5745 and 138 nM for the interaction with the E34QCaM. The drastically reduced affinity of Ca_V1 peptides for E12QCaM and E34QCaM indicates reduced Ca^{2+} binding affinity of each lobe of CaM.

Condensed Versus Extended Conformations of CaM Bound to Peptides—We next used FRET to evaluate proximity of the lobes of CaM to each other when bound to the peptides. We mutated CaM, E12QCaM, and E34QCaM at positions 34 and 110 to place cysteines for labeling with FRET reagents, IAEDNS, and DDPM. DDPM is a nonfluorescent energy-trans-

TABLE 6

Magnitude of fluorescence quenched by peptide relative to CaM molecule labeled with donor and acceptor without peptide

Values in parentheses are (*n*-numbers).

	CaM^{DA}	CaM^{D}	$E12Q^{DA}$	$E12Q^{D}$	$E34Q^{DA}$	$E34Q^{D}$
No peptide	1.00 ± 0.02 (8)	1.00 ± 0.09 (9)	1.00 ± 0.03 (9)	1.00 ± 0.07 (9)	1.00 ± 0.04 (9)	1.00 ± 0.05 (9)
$Ca_V1.1$ IQ	0.58 ± 0.06[a](6)	1.46 ± 0.08[a](6)	1.00 ± 0.07 (7)	1.12 ± 0.05[a](8)	1.03 ± 0.03 (6)	1.18 ± 0.06[a](6)
$Ca_V1.1$ IQH1532Y	0.59 ± 0.03[a](6)	1.53 ± 0.13[a](6)	1.04 ± 0.24 (6)	1.29 ± 0.16[a](6)	0.99 ± 0.02 (6)	1.40 ± 0.06[a](6)
$Ca_V1.1$/H1532Y/M1537K	0.57 ± 0.04[a](6)	1.46 ± 0.11[a](6)	0.97 ± 0.04 (6)	1.08 ± 0.08 (6)	0.83 ± 0.03[a](6)	1.28 ± 0.12[a](6)
$Ca_V1.1$/H1532Y/Q1540K)	0.58 ± 0.04[a](3)	1.50 ± 0.06[a](3)	0.99 ± 0.03 (3)	1.19 ± 0.08 (3)	0.78 ± 0.03[a](3)	1.33 ± 0.04[a](3)
$Ca_V1.1$/H1532Y/E1542Q	0.60 ± 0.01[a](3)	1.52 ± 0.08[a](3)	0.92 ± 0.17 (5)	1.32 ± 0.16[a](6)	0.87 ± 0.04[a](3)	1.29 ± 0.02[a](3)
$Ca_V1.1$/H1532Y/M1537K/Q1540K	0.58 ± 0.07[a](8)	1.44 ± 0.10[a](8)	0.98 ± 0.03 (8)	1.11 ± 0.10 (8)	0.78 ± 0.05[a](8)	1.23 ± 0.08[a](8)
$Ca_V1.2$ IQ	0.58 ± 0.05[a](6)	1.45 ± 0.11[a](6)	0.93 ± 0.04[a](8)	1.11 ± 0.07[a](9)	0.74 ± 0.03[a](6)	1.14 ± 0.18 (6)
$Ca_V1.2$ IQ/Y1675H	0.59 ± 0.06[a](6)	1.42 ± 0.14[a](6)	1.00 ± 0.06 (6)	1.09 ± 0.10 (6)	0.83 ± 0.13 (6)	1.20 ± 0.13[a](6)

[a] *p* value<0.01 by Student's *t* test compares CaM with peptide to CaM with no peptide.

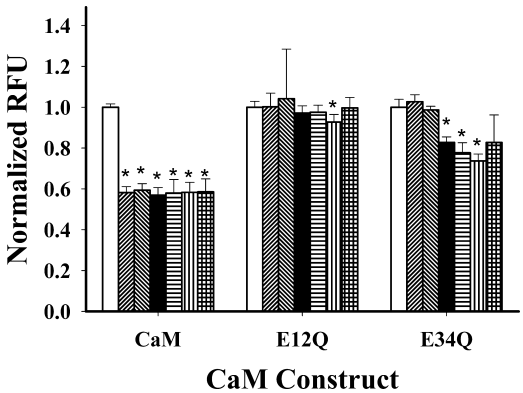

FIGURE 7. **FRET to compare ability of peptides to bind both lobes of CaM.** CaM and peptide concentrations were 200 nM and 2 μM, respectively. *Bars* represent data from cysteine mutant CaMs labeled with both donor and quenching acceptor. In all CaM groups, *empty bars* indicate no peptide; *forward slanting diagonal lines* indicate $Ca_V1.1$ IQ peptide; *backward slanting diagonal lines* indicate $Ca_V1.1$ H1532Y peptide; *filled bars* indicate $Ca_V1.1$/H1532Y/M1537K peptide; *horizontal lines* indicate $Ca_V1.1$/H1532Y/M1537K/Q1540K peptide; *vertical lines* indicate $Ca_V1.2$ IQ peptide; *cross-hatched lines* indicate $Ca_V1.2$ Y1675H. (*, *p* value <0.005 compared with no peptide.)

fer acceptor with IAEDNS as the donor. Residues 34 and 110 of CaM face the solvent in nearly all known structures of CaM and are usually far from the ligand-binding sites. A decrease in the donor fluorescence indicates FRET, as measured relative to CaM labeled with only the donor fluorophore. When fluorescence is decreased in the presence of peptide, the lobes of CaM are closer together. When CaM is labeled with both donor and acceptor (CaM^{DA}), the FRET in the presence of Ca^{2+} is greater in the presence of the IQ than in its absence (Table 6). The peptides alone increase the fluorescence of CaM^{D}, suggesting that the fluorescence of the donor is somewhat influenced by the peptide under the presented conditions. However, as shown in Table 6, the peptide effects on CaM^{D} fluorescence are not responsible for the FRET with CaM^{DA} and therefore do not affect the ability of the acceptor to quench donor fluorescence. The data summarized in Table 6 indicate that fully Ca^{2+}-bound CaM^{DA} binds to the Cav1.1 IQ and Cav1.2 IQ peptides and assumes a compact conformation with the two lobes in close proximity (Fig. 7 and Table 6). FRET signals were also obtained with both E12QCaM-$Ca_V1.2$ IQ and E34QCaM-Cav1.2 IQ (Fig. 7 and Table 6). In contrast, neither the E12QCaM-$Ca_V1.1$ IQ nor the E34QCaM-$Ca_V1.2$ IQ complex displayed FRET, suggesting that partially saturated CaM does not assume a compact configuration when bound to $Ca_V1.1$ IQ. If the Y1675H substitution is made in the $Ca_V1.2$ peptide, no FRET was obtained with E34QCaM, indicating that this substitution alters the interaction with the apo-form of the C-lobe. No FRET was detected with E34Q and the $Ca_V1.1$ IQ peptide with H1532Y substitution, suggesting this residue alone cannot account for the interaction with the Ca^{2+}-free C-lobe. However, the absence of FRET response could be due to the conformation of the $Ca_V1.1$ H1532Y peptide (see supporting information). Conversion of other $Ca_V1.1$ amino acids to the corresponding ones in $Ca_V1.2$ IQ produced increased FRET values similar to E34Q/$Ca_V1.2$ IQ (Fig. 7).

DISCUSSION

One mechanism that would allow CaM to regulate the response of different target proteins to different Ca^{2+} signals is for the binding sites themselves to regulate the Ca^{2+} affinity of the bound CaM. We provide evidence for this mechanism by demonstrating that subtle differences in CaM-binding sites of $Ca_V1.1$ and $Ca_V1.2$ lead to differences in the Ca^{2+} binding properties of the lobes of CaM. Assuming these findings accurately reflect Ca^{2+} sensing by CaM bound to L-type Ca^{2+} channels, then calmodulin modulation of $Ca_V1.2$ channels would be expected to be more sensitive to Ca^{2+} than that of $Ca_V1.1$ channels. In $Ca_V1.2$, the tyrosine at residue 1675 has contact with methionines in the C-lobe of CaM and also interacts through a hydrogen bond involving a water molecule and the C-lobe backbone. This difference in conformation compared with CaM in complex with $Ca_V1.1$ is likely to contribute to the higher affinity of $Ca_V1.2$ IQ for CaM. In $Ca_V1.1$ the histidine (His-1532) in place of the tyrosine is likely to increase the flexibility of the 3–4 loop of CaM and Phe-1533 of $Ca_V1.1$ IQ, resulting in fewer stabilizing interactions and lower affinity. The amino acid in this position (Tyr-1674 in $Ca_V1.2$ and His-1532 in $Ca_V1.1$) is obviously important for affinity of CaM for the peptide, but it does not fully account for differences in the Ca^{2+} affinity of CaM bound to peptides. Our data suggest that the other three amino acids that differ between these two peptides and do not directly contact CaM when CaM is fully Ca^{2+}-saturated participate in the binding of CaM that has one or both lobes Ca^{2+}-free. This argues that different conformations of CaM bind to $Ca_V1.2$. Although several studies from other laboratories have shown that the Ca^{2+} affinity of CaM is influenced by binding to different targets (34, 38–41), we elucidated the contributions of the nonconserved amino acids within the IQ-binding site responsible for this effect on Ca^{2+} affinity, and we demonstrated that these amino acids play a role in regulating the apparent Ca^{2+} affinity by modulating the interactions with CaM with at least one lobe Ca^{2+}-free. Additional contri-

butions from channel sequence outside the IQ-binding site studied in this work are likely to contribute to CaM interactions. Recent structural data from $Ca_V1.2$ (42) and biochemical studies with longer peptides from both $Ca_V1.1$ and $Ca_V1.2$ channels (43) suggest that CaM interacts with the "pre-IQ" regions. Thus differences in these regions could play a role in the difference between the $Ca_V1.1$ and $Ca_V1.2$ channel interactions with CaM.

In the Ca^{2+}-CaM/$Ca_V1.2$ structure, Lys-1680 contacts the C-lobe through a water molecule. A question arising from the differences in affinity of $Ca_V1.1$ and $Ca_V1.2$ for Ca^{2+}-CaM is whether the $Ca_V1.2$ IQ lysines electrostatically attract the negatively charged CaM. CaM is an acidic protein with a net negative charge (−16e) and a calculated pI of 4.15 (44). The peptide $Ca_V1.2$ IQ has a +3 greater net charge over $Ca_V1.1$ IQ, having theoretical pI values of 10.12 and 9.52, respectively. The salinity of the solvent and the positive charges on the peptides may stabilize the compact conformation of the CaM allowing its negatively charged lobes to be close together (45).

Although the parallel arrangement of the N- and C-lobes of CaM bound to $Ca_V1.1$ IQ peptide presented here is in agreement with the arrangement seen with the $Ca_V1.2$ IQ and other peptides (28, 35, 36), it is opposite to the structure of three Ca_V2 IQ-Ca^{2+}CaM complexes reported by Kim *et al.* (46). In these structures CaM is bound in an anti-parallel arrangement, with the N-lobe of CaM binding the carboxyl terminus of the Ca_V2-IQ peptide and the C-lobe binding the amino terminus of Ca_V2-IQ.

Our data suggest that CaM has the ability to bind to $Ca_V1.2$ IQ, in both a fully and a partially Ca^{2+}-saturated state with higher affinity than to $Ca_V1.1$. Recently Saucerman and Bers (47) suggested that the affinity of proteins for CaM determines their response to local Ca^{2+} signals. In the case of the Ca_V1 channels discussed here, the different affinities of skeletal and cardiac isoforms for fully or partially Ca^{2+}-saturated CaM could indicate selective modulation and fine-tuning of local Ca^{2+}-dependent pathways or more specifically their CDI and CDF.

In the case of the $Ca_V1.2$ channel, it has been suggested that the Ca^{2+}-C-lobe CaM interaction is important for CDI (11), whereas the Ca^{2+}-N-lobe interaction participates in the CDF (35, 36). Given the similarity in the structural arrangement of $Ca_V1.1$ IQ and $Ca_V1.2$ IQ complexes with CaM, similar responses are expected for $Ca_V1.1$. Furthermore, because the nonconserved amino acids between $Ca_V1.1$ IQ and $Ca_V1.2$ IQ domains are involved in the interactions with CaM C-lobe, both $Ca_V1.1$ IQ and $Ca_V1.2$ IQ domains are expected to have similar response to CDF, which is modulated by the CaM N-lobe.

The Ca^{2+} titration of the fluorescence of F92WCaM in complex with $Ca_V1.2$ shows evidence of two components (increase followed by a decrease in fluorescence with increasing Ca^{2+}). Substitution of any of the amino acids in $Ca_V1.2$ for those in $Ca_V1.1$ eliminates the second phase fluorescence quenching, suggesting that all of these amino acids contribute to this second Ca^{2+}-dependent event. The biphasic Ca^{2+} response of F92WCaM bound to $Ca_V1.2$ IQ is best explained by the binding of Ca^{2+} at the C-lobe at Ca^{2+} concentrations less than 100 nM followed by a change in the environment of the tryptophan at amino acid 92 (reflected by a quenching of the fluorescence) when Ca^{2+} binds to the N-lobe. The ability of the Trp-92 to sense Ca^{2+} binding to both lobes may reflect its location in the linker helix that connects the lobes. The tryptophan at position 19 in the N-lobe is less likely to sense Ca^{2+} binding at the C-lobe because it is not directly connected to the linker helix. A two-phase Ca^{2+} equilibrium curve is not apparent when F92W binds to $Ca_V1.1$ IQ.

Indirect Ca^{2+} dissociation data with F92W also reveal a stable Ca^{2+} intermediate state for CaM binding to $Ca_V1.2$ IQ that is not seen with $Ca_V1.1$ IQ. During Ca^{2+} dissociation, the fluorescence of F92W first increases then decreases (1), suggesting that Ca^{2+} dissociates first from the N-lobe relieving the fluorescence quenching and then dissociates more slowly from the C-lobe. These data again support the existence of a stable intermediate state of CaM with the C-lobe Ca^{2+}-bound and the N-lobe Ca^{2+}-free. This state is likely to exist in a cell when the Ca^{2+} concentration is declining after a transient. The question becomes what is the functional role of this intermediate state? A Ca^{2+}-binding site mutant that cannot bind Ca^{2+} at the N-lobe still supports Ca^{2+}-dependent inactivation of this channel, and hence the role of this intermediate form may be to help to close or inactivate the channel. The FRET data suggest that CaM can also interact with $Ca_V1.2$ in a compact conformation with the C-lobe Ca^{2+}-free and the N-lobe Ca^{2+}-bound. This would be expected to be the first change in CaM bound to the channel when Ca^{2+} begins to rise in a cell at the start of the Ca^{2+} transient. Yue and co-workers (2) suggested that Ca^{2+} binding to the N-lobe drives Ca^{2+}-dependent facilitation. We conclude that CaM with intermediate saturation states can assume very different conformations depending on whether the N- or C-lobe is Ca^{2+}-bound and in doing so may produce very different functional outcomes.

The IQ motif is likely to be at least part of the binding site for apoCaM (Ca^{2+}-free CaM) (1, 9, 13, 25), but the amino acid residues involved in the binding of apoCaM have not yet been identified. Our data suggest that at least with the partially Ca^{2+}-saturated states the apo-N-lobe and the apo-C-lobe can bind within the IQ sequence of $Ca_V1.2$, and the residues at positions Tyr-1675, Lys-1680, Lys-1683, and Gln-1685 contribute to the interaction. A more detailed analysis of CaM interactions with larger regions of the C-tail is needed to determine how CaM can move within its binding pocket upon binding Ca^{2+}. In addition other parts of the channel itself may interact near or with the IQ motif. A recent report by Dick *et al.* (48) suggests that the N-lobe of a single CaM molecule switches to an amino-terminal site on the Ca_V1 channels. CaM binding could either promote or inhibit protein-protein interactions.

Our previous studies and those of Van Petegem *et al.* (36) suggest that CaM is most likely binding with both lobes Ca^{2+} saturated to determinants within the IQ motif during CDF rather than CDI (28, 36). The data presented here provide the tools needed to test this hypothesis by providing a means to alter the Ca^{2+} sensitivity of CaM. Our studies also provide details of how the binding site itself regulates the affinity of EF

hands of CaM for Ca^{2+} and identifies new interactions that contribute to CaM binding to the IQ motif.

Acknowledgments—We thank Drs. Henry Bellamy and David Neau for their services at the Center for Advanced Microstructures and Devices Gulf Coast Protein Crystallography Consortium beamline. We also thank Dr. Timothy Palzkill for access to the Biacore3000.

REFERENCES

1. Black, D. J., Halling, D. B., Mandich, D. V., Pedersen, S. E., Altschuld, R. A., and Hamilton, S. L. (2005) *Am. J. Physiol. Cell Physiol.* **288,** C669–676
2. Tadross, M. R., Dick, I. E., and Yue, D. T. (2008) *Cell* **133,** 1228–1240
3. Houdusse, A., Gaucher, J. F., Krementsova, E., Mui, S., Trybus, K. M., and Cohen, C. (2006) *Proc. Natl. Acad. Sci. U.S.A.* **103,** 19326–19331
4. Drum, C. L., Yan, S. Z., Bard, J., Shen, Y. Q., Lu, D., Soelaiman, S., Grabarek, Z., Bohm, A., and Tang, W. J. (2002) *Nature* **415,** 396–402
5. Meador, W. E., Means, A. R., and Quiocho, F. A. (1992) *Science* **257,** 1251–1255
6. Meador, W. E., Means, A. R., and Quiocho, F. A. (1993) *Science* **262,** 1718–1721
7. Schumacher, M. A., Rivard, A. F., Bächinger, H. P., and Adelman, J. P. (2001) *Nature* **410,** 1120–1124
8. Elshorst, B., Hennig, M., Försterling, H., Diener, A., Maurer, M., Schulte, P., Schwalbe, H., Griesinger, C., Krebs, J., Schmid, H., Vorherr, T., and Carafoli, E. (1999) *Biochemistry* **38,** 12320–12332
9. Erickson, M. G., Liang, H., Mori, M. X., and Yue, D. T. (2003) *Neuron* **39,** 97–107
10. Pate, P., Mochca-Morales, J., Wu, Y., Zhang, J. Z., Rodney, G. G., Serysheva, I. I., Williams, B. Y., Anderson, M. E., and Hamilton, S. L. (2000) *J. Biol. Chem.* **275,** 39786–39792
11. Peterson, B. Z., DeMaria, C. D., Adelman, J. P., and Yue, D. T. (1999) *Neuron* **22,** 549–558
12. Pitt, G. S., Zühlke, R. D., Hudmon, A., Schulman, H., Reuter, H., and Tsien, R. W. (2001) *J. Biol. Chem.* **276,** 30794–30802
13. Tang, W., Halling, D. B., Black, D. J., Pate, P., Zhang, J. Z., Pedersen, S., Altschuld, R. A., and Hamilton, S. L. (2003) *Biophys. J.* **85,** 1538–1547
14. Zühlke, R. D., Pitt, G. S., Deisseroth, K., Tsien, R. W., and Reuter, H. (1999) *Nature* **399,** 159–162
15. Stroffekova, K. (2008) *Pfluegers Archiv.* **455,** 873–884
16. Liang, H., DeMaria, C. D., Erickson, M. G., Mori, M. X., Alseikhan, B. A., and Yue, D. T. (2003) *Neuron* **39,** 951–960
17. Kim, J., Ghosh, S., Nunziato, D. A., and Pitt, G. S. (2004) *Neuron* **41,** 745–754
18. Kobrinsky, E., Schwartz, E., Abernethy, D. R., and Soldatov, N. M. (2003) *J. Biol. Chem.* **278,** 5021–5028
19. Hudmon, A., Schulman, H., Kim, J., Maltez, J. M., Tsien, R. W., and Pitt, G. S. (2005) *J. Cell Biol.* **171,** 537–547
20. Mouton, J., Ronjat, M., Jona, I., Villaz, M., Feltz, A., and Maulet, Y. (2001) *FEBS Lett.* **505,** 441–444
21. Sencer, S., Papineni, R. V., Halling, D. B., Pate, P., Krol, J., Zhang, J. Z., and Hamilton, S. L. (2001) *J. Biol. Chem.* **276,** 38237–38241
22. Xiong, L., Zhang, J. Z., He, R., and Hamilton, S. L. (2006) *Biophys. J.* **90,** 173–182
23. Dolmetsch, R. E., Pajvani, U., Fife, K., Spotts, J. M., and Greenberg, M. E. (2001) *Science* **294,** 333–339
24. Black, D. J., Tikunova, S. B., Johnson, J. D., and Davis, J. P. (2000) *Biochemistry* **39,** 13831–13837
25. Xiong, L., Kleerekoper, Q. K., He, R., Putkey, J. A., and Hamilton, S. L. (2005) *J. Biol. Chem.* **280,** 7070–7079
26. Xiong, L. W., Newman, R. A., Rodney, G. G., Thomas, O., Zhang, J. Z., Persechini, A., Shea, M. A., and Hamilton, S. L. (2002) *J. Biol. Chem.* **277,** 40862–40870
27. Rodney, G. G., Williams, B. Y., Strasburg, G. M., Beckingham, K., and Hamilton, S. L. (2000) *Biochemistry* **39,** 7807–7812
28. Fallon, J. L., Halling, D. B., Hamilton, S. L., and Quiocho, F. A. (2005) *Structure* **13,** 1881–1886
29. Otwinowski, Z., and Minor, W. (1997) *Methods Enzymol.* **276,** 307–326
30. Rossmann, M. G. (1972) *The Molecular Replacement Method,* (Rossman, M. G., ed) Gordon and Breach Science Publishers, Inc., New York
31. Brünger, A. T., Adams, P. D., Clore, G. M., DeLano, W. L., Gros, P., Grosse-Kunstleve, R. W., Jiang, J. S., Kuszewski, J., Nilges, M., Pannu, N. S., Read, R. J., Rice, L. M., Simonson, T., and Warren, G. L. (1998) *Acta Crystallogr. D Biol. Crystallogr.* **54,** 905–921
32. Sack, J. S., and Quiocho, F. A. (1997) *Methods Enzymol.* **277,** 158–173
33. Rovati, G. E., and Nicosia, S. (1994) *Trends Pharmacol. Sci.* **15,** 140–144
34. Johnson, J. D., Snyder, C., Walsh, M., and Flynn, M. (1996) *J. Biol. Chem.* **271,** 761–767
35. Mori, M. X., Vander Kooi, C. W., Leahy, D. J., and Yue, D. T. (2008) *Structure* **16,** 607–620
36. Van Petegem, F., Chatelain, F. C., and Minor, D. L., Jr. (2005) *Nat. Struct. Mol. Biol.* **12,** 1108–1115
37. Mukherjea, P., Maune, J. F., and Beckingham, K. (1996) *Protein Sci.* **5,** 468–477
38. Bayley, P. M., Findlay, W. A., and Martin, S. R. (1996) *Protein Sci.* **5,** 1215–1228
39. Gaertner, T. R., Putkey, J. A., and Waxham, M. N. (2004) *J. Biol. Chem.* **279,** 39374–39382
40. Olwin, B. B., and Storm, D. R. (1985) *Biochemistry* **24,** 8081–8086
41. Peersen, O. B., Madsen, T. S., and Falke, J. J. (1997) *Protein Sci.* **6,** 794–807
42. Fallon, J. L., Baker, M. R., Xiong, L., Loy, R. E., Yang, G., Dirksen, R. T., Hamilton, S. L., and Quiocho, F. A. (2009) *Proc. Natl. Acad. Sci. U.S.A.* **106,** 5135–5140
43. Ohrtman, J., Ritter, B., Polster, A., Beam, K. G., and Papadopoulos, S. (2008) *J. Biol. Chem.* **283,** 29301–29311
44. Walker, S. W., Wark, J. D., MacNeil, S., Mellersh, H., Brown, B. L., and Tomlinson, S. (1984) *Biochem. J.* **217,** 827–832
45. André, I., Kesvatera, T., Jönsson, B., and Linse, S. (2006) *Biophys. J.* **90,** 2903–2910
46. Kim, E. Y., Rumpf, C. H., Fujiwara, Y., Cooley, E. S., Van Petegem, F., and Minor, D. L., Jr. (2008) *Structure* **16,** 1455–1467
47. Saucerman, J. J., and Bers, D. M. (2008) *Biophys. J.* **95,** 4597–4612
48. Dick, I. E., Tadross, M. R., Liang, H., Tay, L. H., Yang, W., and Yue, D. T. (2008) *Nature* **451,** 830–834